

Estimating diameters of pulmonary nodules with competition-diffusion and robust ellipsoid fit

Toshiro Kubota¹ and Kazunori Okada²

¹ CAD Solutions, Siemens Medical Solutions

² Real-Time Vision & Modeling department, Siemens Corporate Research

Abstract. We propose a new technique to extract a pulmonary nodule from helical thoracic CT scans and estimate its diameter. The technique is based on a novel segmentation, or label-assignment, framework called competition-diffusion (CD), combined with robust ellipsoid fitting (EF). The competition force defined by replicator equations draws one dominant label at each voxel, and the diffusion force encourages spatial coherence in the segmentation map. CD is used to reliably extract foreground structures, and nodule like objects are further separated from attached structures using EF. Using ground-truth measured manually over 1300 nodules taken from more than 240 CT volumes, the performance of the proposed approach is evaluated in comparison with two other techniques: Local Density Maximum algorithm and the original EF. The results show that our approach provides the most accurate size estimates.

1 Introduction

Measuring the size of pulmonary nodules from X-ray computed tomography (CT) data is an important practice for diagnosis and progression analysis of lung cancer. The nodule size often plays an important role in choosing a proper patient care, and is also an effective feature to separate true nodules from nodule-like spurious findings. Typically, the size is represented by the diameter of the nodule. In clinical practice, it is conventional to use the 2D diameter-based estimation because the manual reading can be done readily by scanning through a CT volume slice by slice. Automating this task for computer-aided diagnosis (CAD) is, however, a difficult problem due to intensity variations, partial volume effects, attachment to other structures, and noise [1–6]. Although a truly 3D based volume estimate may give more accurate information for diagnosis and prognosis, we anticipate the trend of the 2D approach will continue for foreseeable future.

A CT-based screening protocol specified by the International Early Lung Cancer Action Program (I-ELCAP) details how the diameter of pulmonary nodules should be measured and how the measurements should be used for determining the patient management. According to the protocol, the result of an initial CT screening of lung is considered positive if at least one solid or part-solid nodule with 5.0mm or more in diameter or at least one non-solid nodule with 8.0mm or more in diameter is found [7]. Although these 5mm and 8mm thresholds are likely to become smaller as more accurate screening becomes possible with high

resolution multi-detector helical CT (MDCT), the importance of nodule size in cancer diagnosis will stay unchanged.

Despite an existing large body of works, nodule segmentation is still an active open problem. More accurate and efficient algorithms will be extremely useful for detection and diagnosis of lung cancer. We consider the segmentation problem in a semi-automated setting where a rough location of a potential nodule is known. There are many candidate detection algorithms that can be used to fully automate our system, in particular as a part of a CAD system. Therefore, our semi-automated treatment does not lessen the importance of the problem and the usefulness of our algorithm.

Recently, a semi-automated size estimation algorithm using a robust Gaussian ellipsoid fitting (EF) was proposed by [8]. Given a marker positioned near a nodule, the algorithm computes the location, orientation and radii of an ellipsoid by fitting a Gaussian-based model to the intensity variation nearby the marker. It employs scale-space mean-shift and a robust scale estimator to find the solution. The volume and diameter of the nodule can be estimated from the ellipsoid. Their work verified the estimation accuracy using a large clinical database [8]. However, the technique tends to be inaccurate in the diameter measurement for small nodules due mainly to the small sample size problem.

The main contribution of this work is a new diameter estimation technique that improves the accuracy and the speed of the original EF. The proposed technique is based on a combination of EF and a technique using *competition-diffusion* segmentation (CD) [9]. The competition-diffusion is a class of reaction-diffusion systems that employ a competitive learning mechanism ([10, 11]) as the system’s reaction term. To our knowledge, this work is the first attempt to apply CD to medical image segmentation problems. It also differs fundamentally from other well-known reaction-diffusion-based segmentation solutions [12, 13]. Our experimental results indicate that CD is highly effective and fast in segmenting solitary nodules, but is not applicable to non-solitary ones. On the other hand, EF is stable and applicable to both solitary and non-solitary nodules, but inaccurate for small solitary ones. Thus, our idea is to apply CD to solitary nodules and EF to non-solitary ones. We use the CD segmentation to determine if the nodule is solitary or non-solitary.

The paper is organized as follows. In Section 2, three segmentation algorithms, CD, EF and Local Density Maximum (LDM) [14], are described. They are compared against the proposed hybrid approach in our experiments. Section 3 describes a diameter estimation technique using the segmentation results. Section 4 introduces the proposed hybrid method (HB). Section 5 shows our experimental results. Section 6 gives summary and concluding remarks.

2 Segmentation

2.1 Competition-Diffusion System

Formulation The goal of the present system is to assign to each location a class label from a set of n classes. We first assign each location a state vector

$\mathbf{x} \in S^n$, where $S^n = \{(x_1, x_2, \dots, x_n) | x_i \geq 0, \sum_i x_i = 1\}$ is called n simplex. Each component in the state vector gives a normalized fitness of the particular class. The closer the state value is to 1, the more fitting the location is to the class. Initially, the class assignment is ambiguous and contaminated with noise in the observation. We then use the competition-diffusion system to filter out the noise and bring one dominant value in the state vector representation at each location. The final segmentation is obtained by assigning the dominant class to each location. The diffusion process brings good spatial coherence to the segmentation map, and the competition process selects the most fitted label and prevents the diffusion process from oversmoothing the state vector representation.

Associated with \mathbf{x} is a spatial coordinate vector $\mathbf{r} \in \Gamma$ where Γ is some manifold in 3-dimension. Let Φ be the space of functions, $\Gamma \rightarrow S^n$, and we consider the following initial value problem.

$$\dot{\mathbf{x}}(\mathbf{r}, t) = \begin{pmatrix} \dot{x}_1(\mathbf{r}, t) \\ \dot{x}_2(\mathbf{r}, t) \\ \vdots \\ \dot{x}_n(\mathbf{r}, t) \end{pmatrix} = \begin{pmatrix} g_1(\mathbf{x}(\mathbf{r}, t)) \\ g_2(\mathbf{x}(\mathbf{r}, t)) \\ \vdots \\ g_n(\mathbf{x}(\mathbf{r}, t)) \end{pmatrix} + \mu \begin{pmatrix} H(\mathbf{x}(\mathbf{r}, t)) \\ H(\mathbf{x}(\mathbf{r}, t)) \\ \vdots \\ H(\mathbf{x}(\mathbf{r}, t)) \end{pmatrix} \quad (1)$$

$$\mathbf{x}(\mathbf{r}, 0) = \mathbf{x}_0 \in \Phi \quad (2)$$

where \dot{x} is the time derivative of x , the first term in the right hand side is a competition term, the second term is a diffusion term, and μ is a positive number that balances the competition term and the diffusion term. We call g_i a component-wise inhibition operator ($g_i : S^n \rightarrow [0, 1]$) and $\mathbf{g} = [g_1, g_2, \dots, g_n]^T$ a competition operator ($G : S^n \rightarrow S^n$). H is a general form of a linear diffusion operator. Our motivation is to encourage spatial homogeneity in the segmentation with the diffusion term and to bring a dominant class at each pixel with the competition term.

We consider a component wise inhibition operator of the following form:

$$g_i(\mathbf{x}) = x_i (f_i(\mathbf{x}) - \bar{f}(\mathbf{x})) \quad (3)$$

where f_i is a fitness function of the i th class, and

$$\bar{f}(\mathbf{x}) = \sum_i x_i f_i(\mathbf{x}) \quad (4)$$

is the average fitness. Equation (3) is often called a replicator equation and has been used to model ecological progression among multiple species. With a suitable choice of the fitness functions, the population of the species reaches an equilibrium state where the multiple species coexist. On the other hand, by choosing another set of fitness functions, we can derive a state where only one species survives or dominates. In our state space representation, it corresponds to the state where $x_i = 1$ and $x_j = 0, \forall j \neq i$. We call this a *mutually exclusive state*. We call the state *internal* when $x_i > 0 \forall i$. For our segmentation problem, we want to derive a state vector representation at each location with one dominant component. We call the state *dominant* when there exists a class whose

state value is strictly the largest. The dominant state may not necessarily be a mutually exclusive one as the diffusion force prevents it from reaching the state at the boundary between different classes.

Let us first list properties of the above initial value problem. Their proof can be found in [15].

- If $\mathbf{x}(0) \in \Phi$, then $\mathbf{x}(t) \in \Phi, \forall t > 0$.
- If f_i is Lipschitz continuous, then the initial value problem of (1) has a unique solution.
- A mutually exclusive state is a stable fixed point if at the fixed point $f_i > f_{j \neq i}$ and $f_i > 0$ where i is the dominant class.
- An internal fixed point is unstable when the fitness function is linear, symmetric and positive definite.

When we use linear fitness function, then the Lipschitz condition is satisfied. The condition of the third item is satisfied if the diagonal elements of the fitness matrix are positive and larger than any of the off-diagonal elements in their respective columns. Thus, to draw a unique solution with a dominant class at every location, we use a linear fitness function with a fitness matrix of \mathbf{M} that is symmetric, positive, and $M_{ii} > M_{ij} \forall i$. The fitness function is

$$f_i(\mathbf{x}) = (\mathbf{M}\mathbf{x})_i \quad (5)$$

with $(\mathbf{v})_i$ being the i th component of a vector \mathbf{v} . The solution gives a dominant class at each location except in degenerate cases when $\mathbf{x}(\mathbf{r})$ reaches a configuration that is constant everywhere and is also a fixed point at every \mathbf{r} .

Nodule Segmentation We use CD to extract nodules, vessels, and other bright foreground structures. For solitary nodules, this step extracts them reliably. For non-solitary nodules, we further apply the robust Gaussian ellipsoid fit to separate nodules from the attached structures.

For nodule segmentation, we provide two classes: background (class 1) and foreground (class 2) that includes nodules, vessels, and other pulmonary structures. Hence $n = 2$. An important design issue for applying CD to a particular segmentation task is the initialization of \mathbf{x} (\mathbf{x}_0 in (1)). we choose the following formula for segmenting pulmonary nodules.

$$x_2(\mathbf{r}) = e^{-2(1-\min(1, I(\mathbf{r})/1000))^2} \quad (6)$$

$$x_1(\mathbf{r}) = 1 - x_2(\mathbf{r}) \quad (7)$$

where $I(\mathbf{r})$ denotes the CT value of the input volume at \mathbf{r} , and 1000 is near the upper CT value of non-calcified pulmonary nodules. Hence for voxels with $I \geq 1000$, $x_2 = 1$ and $x_1 = 0$. For voxels with $I < 1000$, x_2 decreases monotonically as I deviates from 1000 while x_1 increases. x_2 takes the minimum value of e^{-2} when $I = 0$. Another design issue is the fitness matrix. We use a 2 by 2 identity matrix which satisfies the above condition for assuring dominant states.

It is convenient to have different time steps for the competition term and the diffusion term in (1). This is equivalent to having spatially variant μ in (1). We use $0.5\bar{f}$ for the time step of the competition term and 0.5 for the diffusion term. Using a linear isotropic diffusion, (1) can be discretized as

$$x_i(\mathbf{r}, n + 1) = 0.5 \frac{x_i(\mathbf{r}, n) f_i(\mathbf{x}(\mathbf{r}, n))}{\bar{f}(\mathbf{x}(\mathbf{r}, n))} + 0.5 \bar{x}_i(\mathbf{r}, n) \quad (8)$$

where \bar{x} is the average value of the six-neighbors. For our experiments, we repeat the iteration for four times, with which one class emerges as a dominant one over the other at each voxel.

2.2 Robust Gaussian Ellipsoid Fit

This technique robustly fits a 3D anisotropic Gaussian function to the nodule’s intensity distribution in a multiscale fashion, given a marker positioned near a target nodule. An ellipsoid that approximates the nodule’s boundary is derived as a specific iso-level or equal-probability contour of the fitted Gaussian. Various nodule size features (e.g., maximum diameter, volume, sphericity) are computed analytically from radii of the ellipsoid. The multiscale analysis is given by i) performing a robust mean shift-based Gaussian model fitting for each of Gaussian scale space images constructed over a set of discrete analysis scales, and ii) find the most stable estimate among the multiscale model estimates by minimizing a form of Jensen Shannon divergence used as a stability criterion. The solution is efficient because the mean shift formulation removes the explicit construction of the Gaussian scale space that are computationally expensive.

At each scale, the nodule center location as Gaussian mean is estimated by the convergence of the scale space mean shift procedures. In the neighborhood of this estimated mean, local data analysis is performed by the mean shift procedures initialized at a set of neighboring points. The anisotropic tumor spread as Gaussian covariance is estimated by a constrained least-squares solution of a linear system constructed with the convergent mean shift vectors. Using information only from the convergent vectors facilitates the robustness, removing outlier samples from the above estimation framework. Due to this, the solution is effective for segmenting wall- or vessel-attached cases. In our experiment, we followed the parameter settings recommended in [8]. The scale space is conceived with 18 analysis scales with 0.25 interval ($0.5^2, \dots, 4.75^2$). And 35% 3D confidence ellipsoid is used for deriving an equal-probability contour from the fitted Gaussian. This confidence threshold was determined experimentally.

2.3 Local Distribution Maximum

The technique applies thresholding at multiple levels followed by connected component analysis on each thresholded volume. It then searches for objects and their *plateaus* in the multiple thresholded volumes. The search starts from the volume with the highest threshold value and moves to ones with lower threshold

values sequentially. A new object is found when a connected component has no overlaps to components in the previous volume. An object becomes a plateau when the ratio between the volume of the object and the volume of its bounding box suddenly decreases by more than some fraction (say η) or the object merges with another plateau. Important parameters of the method are the threshold values and η . In our experiment, we set $\eta = 1/30$ following the recommendation in [14] and set 12 threshold levels between 0 and 1100 with an increment of 100.

3 Diameter Estimation

According to the I-ELCAP protocol [7], "the diameter of a nodule is estimated as the average length and width where length is measured on a single CT image that shows the maximum length; and width is defined as the longest perpendicular to the length." Typically, the CT image is selected along the axial direction, due mainly to high-resolution and isotropic nature of the axial view. We follow closely with the protocol to estimate the diameter from the segmentation.

For LDM and CD, the diameter of a nodule is estimated as follows. After the segmentation and connected component analysis, the component that is closest to the marker is selected as the target nodule. In most cases, the marker is contained within the component, but in some cases, it lies on the background due to inaccurate marker positioning. Next, the component is analyzed slice by slice in the axial view. For each axial slice, 2-dimensional connected component analysis is performed, an ellipse is fitted to each component, and the geometrical mean of the axes is recorded for each ellipse. Among all 2-dimensional connected components, we select the one with the maximum geometrical mean for diameter measurement. The diameter is then estimated as the average width and height of the bounding box enclosing the selected component. Use of the geometrical mean instead of an arithmetic mean gives a slightly better agreement with the ground-truth.

For EF, the diameter is estimated as follows. First, an ellipsoid directly derived from the estimated covariance is projected on the axial plane, and then the radii of the ellipse on the projection plane is computed. The diameter is estimated as the arithmetic mean of the radii times the scaling constant of 1.6416, corresponding to the 35% confidence limit.

4 Hybrid Method

When a nodule is attached to another structure, CD will segment both of them together and result in a large over-estimated volume. This segmented volume usually stretches out to the boundary of the bounding volume (21x21x21 in our experiments). This observation leads to a simple test for the nodule type. If the segmentation volume touches one of six boundaries of the bounding volume, it is considered non-solitary. Otherwise, it is considered solitary. We can also compute the ratio between the segmentation volume and the volume of the bounding box enclosing the segmentation to check if the segmentation has a

reasonably spherical shape. In our experiments, we only used the boundary check to determine if the nodule is solitary.

By using this solitary/non-solitary check of a nodule with CD segmentation, we implement a hybrid approach to the diameter estimation problem. For each given marker, a sub-volume of $21 \times 21 \times 21$ voxels is extracted. CD segmentation is then applied to the volume, followed by the boundary check. If the boundary check indicates the nodule to be solitary, we apply the diameter estimation by the CD segmentation. Otherwise, we apply EF on the sub-volume and estimate the diameter. This hybrid approach is denoted by HB in the rest of the paper.

5 Experiments

In this section, we evaluate the performance of HB in comparison to EF, LDM and CD. We use 1349 nodules taken from over 240 CT volumes for the evaluation. Certified radiologists placed markers by eye-appraisal, resulting in at least one marker for each nodule. A $21 \times 21 \times 21$ bounding volume is used as an input. The ground-truth diameter for each nodule is measured by human experts (both radiologists and scientists in the medical imaging field) following the IELCAP protocol.

First, we qualitatively evaluate the segmentation results of EF, LDM and CD. Figures 5(a)-(l) show some illustrative examples of segmentation results and their diameter estimates. In each figure, the left, middle and right images are the result's axial slices for EF, LDM and CD, respectively. The location of the slice is at the center of the ellipsoid computed by EF. The EF results are displayed by an ellipse (conic) on the cutting plane with the original data superimposed. The first number at the top-left corner is the ground-truth and the second number is the EF's estimate. The numbers in the LDM and CD results are the respective estimates.

As stated in Section 1, EF has difficulties in processing small nodules. This is observed in Figures 5(g)-(h). EF can also segment a part of the surrounding background as a nodule, leading to an over-estimation of the diameter as shown in Figure 5(h). A problem associated with LDM is its sensitivity to the pre-determined threshold levels, which are typically set by a fixed increment. The segmentation of an object becomes inaccurate when the intensity distribution of the object has an overlap with the distribution of its plateau. This can be observed in Figures 5(i)-(j). The degree and the frequency of the problem can be reduced by increasing the number of threshold levels, but at the cost of increasing the computational load. CD is effective in estimating the diameter of solitary nodules. However, the technique is not applicable to nodules attached to other structures such as the lung wall as seen in Figures 5(k)-(l).

Next, the estimation accuracy is quantitatively evaluated with the ground-truth. According to the CD-based boundary test, there are 614 solitary and 735 non-solitary nodules in the data set. We first evaluate the performance of EF, LDM and CD separately for the two types of nodules. The squared difference between the estimates and the corresponding ground-truth is used as error met-

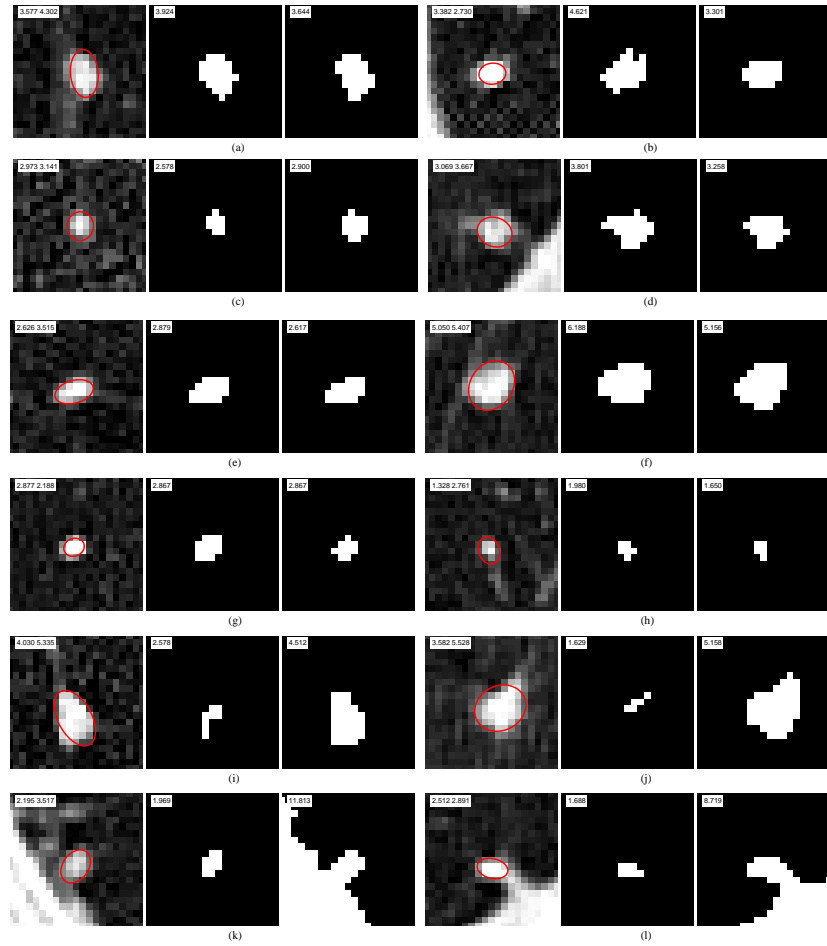


Fig. 1. Results of segmentation algorithms.

ric. Figures 2-3 show the results for solitary and non-solitary cases, respectively. The mean is shown in log scale to improve the visibility of the plots while the deviation is shown in linear scale. The error statistics are computed as a function of the diameter sampled discretely between 1 and 7 with a 0.5mm interval. The mean and standard deviation are computed in a ± 0.5 range for each of the center diameter.

For solitary nodules, the error tends to positively correlate with the diameter. Thus the squared difference error can be normalized by the corresponding center diameter for better interpretation. CD is more accurate than EF and LDM across all sizes except at 3mm where LDM with 0.2913 normalized-error is slightly better than CD with 0.2972 normalized-error. For non-solitary nodules, CD is the least accurate and EF is the most accurate one. For EF and CD, the error

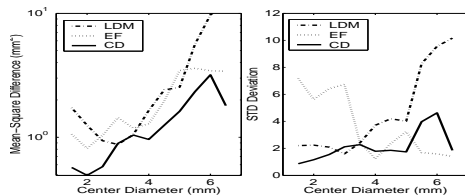


Fig. 2. Estimation performance of EF, LDM and CD for solitary nodules.

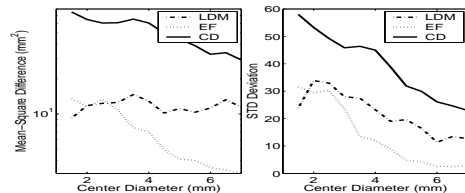


Fig. 3. Estimation performance of EF, LDM and CD for non-solitary nodules.

tends to negatively correlate with the diameter while it stays around $2.5mm^2$ for LDM. The large error by CD is due to the over-segmentation problem.

Next, the performance of HB is evaluated using both nodule types together. Figure 4 shows the mean and the standard deviation of the squared difference errors in linear scale for EF, LDM and HB using the same diameter ranges as in Figures 2-3. HB constantly gives a smaller error than other methods in all sizes. This is not a surprising result; HB analyzes the solitary and non-solitary nodules by CD and EF whose accuracy in their respective categories has been verified above. Table 6 summarizes the computational efficiency of each estimation technique computed as the mean and standard deviation over 1349 nodules. The results indicate that CD is computationally most efficient while EF is most expensive. HB is about 50% faster than EF.

6 Conclusion

We introduced a new pulmonary nodule size/diameter estimation technique that combined robust Gaussian ellipsoid fit (EF) and competition-diffusion segmentation (CD). The technique first uses CD to separate foreground structures from the background, and applies EF if necessary to separate a nodule from attachment. If the nodule is solitary, the CD step alone is sufficient. A simple test on the CD segmentation accurately separates solitary and non-solitary cases.

Our experiments show that this hybrid method outperforms EF, CD and Local Density Maximum. For solitary nodules (see Figure 2), the mean-square difference error between the estimates and the ground-truth is $1.19 mm^2$ with EF and $0.73 mm^2$ with CD: a 35% reduction. The hybrid method is also twice as fast as EF.

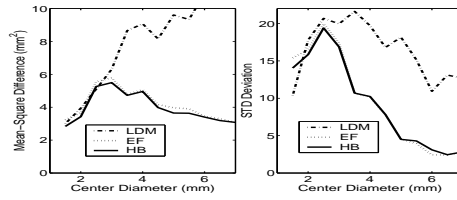


Fig. 4. Performance of EF, LDM and HB for both solitary and non-solitary nodules.

Table 1. Comparison of Computation Time (seconds)

Method	EF	LDM	CD	HB
mean	1.26	0.269	0.0510	0.651
std	0.25	0.18	0.014	0.7

References

1. van Ginneken, B., ter Harr Romeny, B.M., Viergever, M.A.: Computer-aided diagnosis in chest radiography: A survey. *IEEE TMI* **20** (2001) 1228–1241
2. Reeves, A.P., Kostis, W.J.: Computer-aided diagnosis of small pulmonary nodules. *Seminars in Ultrasound, CT, and MRI* **21** (2000) 116–128
3. Ko, J.P., Naidich, D.P.: Computer-aided diagnosis and the evaluation of lung disease. *J. Thorac Imaging* **19** (2004) 136–155
4. Armato, S., et al.: Computerized detection of pulmonary nodules on CT scans. *RadioGraphics* **19** (1999) 1303–1311
5. Fan, L., Novak, C., Qian, J., Kohl, G., Naidich, D.: Automatic detection of lung nodules from multi-slice low-dose CT images. In: *SPIE Med. Imag.* (2001)
6. Lee, Y., et al.: Automated detection of pulmonary nodules in helical CT images based on an improved template-matching technique. *IEEE TMI* **20** (2001) 595–604
7. Henschke, C.I., et al.: CT screening for lung cancer: Frequency and significance of part-solid and nonsolid nodules. *Am. J. Roentgen.* **178** (2002) 1053–1057
8. Okada, K., Comaniciu, D., Krishnan, A.: Robust anisotropic Gaussian fitting for volumetric characterization of pulmonary nodules in multislice CT. *IEEE TMI* **24** (2005) 409–423
9. Kubota, T., Espinal, F.: Reaction-diffusion systems for hypothesis propagation. In: *ICPR00.* (2000) Vol III: 547–550
10. Pelillo, M.: The dynamics of nonlinear relaxation labeling processes. *Journal of Mathematical Imaging and Vision* **7** (1997) 309–323
11. Carpenter, G.A., Grossberg, S.: A massively parallel architecture for a self-organizing neural pattern recognition machine. *Computer Vision, Graphics, and Image Processing* **37** (1987) 54–115
12. Tek, H., Kimia, B.: Volumetric segmentation of medical images by three-dimensional bubbles. *CVIU* **64** (1997) 246–258
13. Zhu, S., Mumford, D.: Prior learning and gibbs reaction-diffusion. *PAMI* **19** (1997) 1236–1250
14. Zhao, B., Gamsu, G., Ginsberg, M.S., Jiang, L., Schwartz, L.H.: Automatic detection of small lung nodules on CT utilizing a local density maximum algorithm. *Journal of Applied Clinical Medical Physics* **4** (2003) 248–260
15. Kubota, T., Okada, K.: Competition-diffusion and its properties. Technical report, Siemens Medical Solutions USA, CAD Solutions (2005)